



A Journal of the Gesellschaft Deutscher Chemiker

# Angewandte Chemie

GDCh

International Edition

www.angewandte.org

## Accepted Article

**Title:** Double Cation- $\pi$ -Driven Strategy Enabling Two-Dimensional Supramolecular Polymers as Efficient Catalyst Carriers

**Authors:** Xuedong Xiao, Hongbo Chen, Xuxu Dong, Dazhuo Ren, Qiang Deng, Dapeng Wang, and Wei Tian

This manuscript has been accepted after peer review and appears as an Accepted Article online prior to editing, proofing, and formal publication of the final Version of Record (VoR). This work is currently citable by using the Digital Object Identifier (DOI) given below. The VoR will be published online in Early View as soon as possible and may be different to this Accepted Article as a result of editing. Readers should obtain the VoR from the journal website shown below when it is published to ensure accuracy of information. The authors are responsible for the content of this Accepted Article.

**To be cited as:** *Angew. Chem. Int. Ed.* 10.1002/anie.202000255  
*Angew. Chem.* 10.1002/ange.202000255

**Link to VoR:** <http://dx.doi.org/10.1002/anie.202000255>  
<http://dx.doi.org/10.1002/ange.202000255>

# Double Cation- $\pi$ -Driven Strategy Enabling Two-Dimensional Supramolecular Polymers as Efficient Catalyst Carriers

Xuedong Xiao,<sup>[a],+</sup> Hongbo Chen,<sup>[b],+</sup> Xuxu Dong,<sup>[a]</sup> Dazhuo Ren,<sup>[a]</sup> Qiang Deng,<sup>[a]</sup> Dapeng Wang,<sup>[b]</sup> and Wei Tian\*<sup>[a]</sup>

[a] X.D. Xiao, X.X. Dong, D.Z. Ren, Q. Deng, Prof. W. Tian  
Shaanxi Key Laboratory of Macromolecular Science and Technology, MOE Key Laboratory of Material Physics and Chemistry under Extraordinary Conditions, School of Chemistry and Chemical Engineering, Northwestern Polytechnical University, Xi'an, 710072, China.  
E-mail: happytw\_3000@nwpu.edu.cn

[b] H.B. Chen, Prof. D.P. Wang  
State Key Laboratory of Polymer Physics and Chemistry, Changchun Institute of Applied Chemistry, Chinese Academy of Sciences, Changchun, Jilin, 130022, China.

\*These authors contribute equally to this work.

**Abstract:** The cation- $\pi$  interaction is a strong non-covalent interaction and can be used to prepare high-strength, stable supramolecular materials. However, because the molecular plane of a cation-containing group and that of aromatic structure are usually perpendicular when forming a cation- $\pi$  complex, it is difficult to exploit the cation- $\pi$  interaction to prepare a 2D self-assembly in which the molecular plane of all the building blocks are parallel. Herein, we propose a "double cation- $\pi$ -driven" strategy to overcome this difficulty and have prepared 2D self-assemblies with long-range ordered molecular hollow hexagons. The double cation- $\pi$  interaction makes the 2D self-assemblies be stable. The 2D self-assemblies are to be an effective carrier that can eliminate metal nanoparticle aggregation. We have demonstrated that such 2D assembly/palladium nanoparticle hybrids exhibit recyclability and superior catalytic activity for a model reaction.

## Introduction

Two-dimensional (2D) materials are attractive in many applications, such as energy storages, optoelectronics, and catalysis.<sup>[1]</sup> Thanks to decades of development, scientists can fabricate sophisticated and ordered 2D supramolecular materials through a bottom-up self-assembly strategy<sup>[2]</sup> that uses small organic molecules<sup>[2b, 2c, 3]</sup> or polymers<sup>[4]</sup> as building blocks. Exploiting this strategy, each building block is self-assembled by taking advantage of various non-covalent interactions, such as metal coordination,<sup>[5]</sup> host-guest,<sup>[6]</sup> hydrophobic effect,<sup>[7]</sup> hydrogen bonding,<sup>[8]</sup> and  $\pi$ - $\pi$  stacking,<sup>[9]</sup> to give structurally well-defined and functional 2D supramolecular materials. Despite tremendous progresses that have been made, it remains a challenge to prepare 2D supramolecular materials with stable structure.

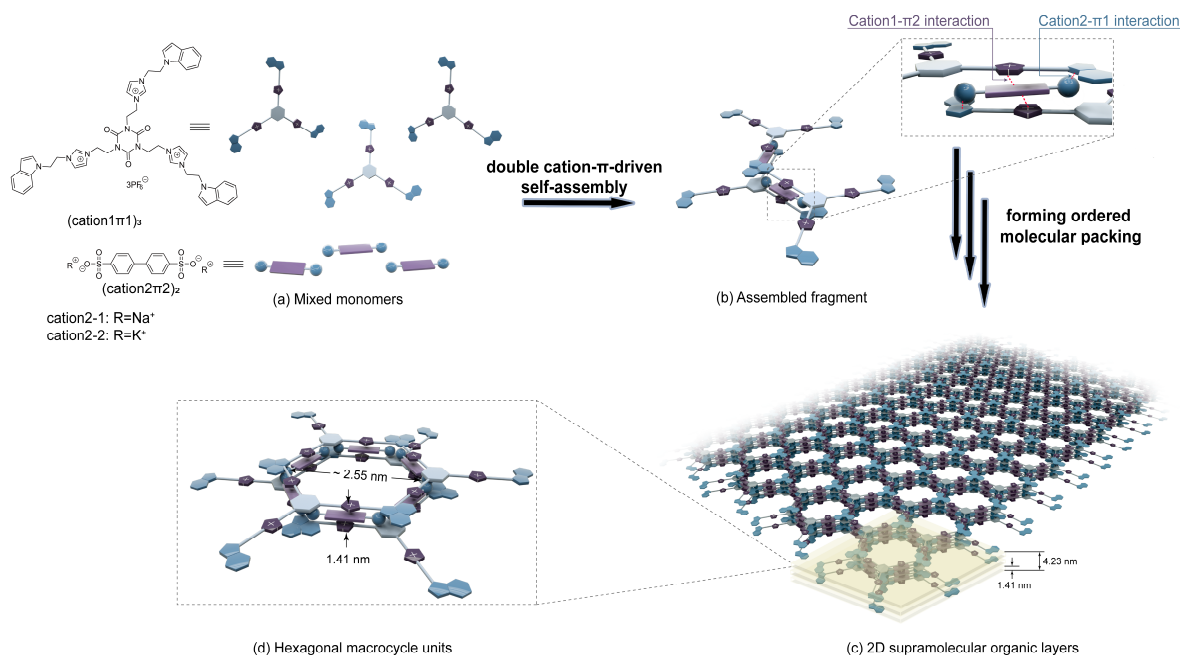
The cation- $\pi$  interaction, involving an electrostatic interaction between a cation and polarizable  $\pi$  electron cloud, is probably the strongest non-covalent interaction.<sup>[10]</sup> Dougherty et al. proposed the term "cation- $\pi$  interaction" in 1990,<sup>[11]</sup> and this type of interaction is known to play an important role in multidisciplinary fields ranging from biology,<sup>[12]</sup> chemistry,<sup>[13]</sup> to material science<sup>[14, 15]</sup> with an evident influence in determining the structure of materials and mediating the function of organisms.<sup>[10b, 16]</sup> Furthermore, in order to form cation- $\pi$  interaction, the molecular plane of cation-containing groups and that of aromatic structure are usually perpendicular.<sup>[10a, 12c]</sup>

However, formation of 2D self-assemblies requires that all building blocks are repetitively arranged in two orthogonal directions.<sup>[2c]</sup> Therefore, it is difficult to prepare stable 2D materials by utilizing the high-strength binding characteristic of the cation- $\pi$  interaction.

In order to avoid the intersection that occurs between the molecular plane of the conjugated  $\pi$ -containing group and that of the neighboring cation-containing group, we proposed a "double cation- $\pi$ -driven" strategy that circumvents this intersection and enables the growth of cation- $\pi$  stabilized materials in two dimensions. To prove this concept, we fabricated 2D supramolecular organic layers (2DSOLs) using the monomers [(cation1 $\pi$ 1)<sub>3</sub> and (cation2 $\pi$ 2)<sub>2</sub>]. The structure of (cation1 $\pi$ 1)<sub>3</sub> monomer consists of a non-aromatic triazine core and three arms having a cation and aromatic groups. The (cation2 $\pi$ 2)<sub>2</sub> monomer composes of biphenyl group and two alkali metal cations Na<sup>+</sup> or K<sup>+</sup>. Importantly, both (cation1 $\pi$ 1)<sub>3</sub> and (cation2 $\pi$ 2)<sub>2</sub> are designed to be 2D (Scheme 1a). This allows the formation of a cation- $\pi$  interaction among the adjacent 2D monomers through edge touch while avoiding intersection (Scheme 1b). The self-assembly direction of monomer is, therefore, expected to be in an epitaxial way in the dimension parallel to the plane of monomers. The epitaxially grown layer can be stacked in the dimension perpendicular to the aforementioned plane (Scheme 1c). The feasibility of such a cation- $\pi$  interaction-driven 2DSOLs is proven by theoretical methods and its formation was confirmed by various experimental techniques. The self-assembled 2DSOLs exhibited high thermal stability and superb solvent resistance. We demonstrated that the 2DSOLs could act as carriers of metal nanoparticles (NPs). Upon using them as catalysts, such hybrids did not only exhibit superior catalytic efficiency relative to the dispersed nanoparticle catalysts, but also be stable, be easily recyclable for resource saving and reduction of waste. Therefore, the double cation- $\pi$ -driven strategy provided new insight into the design of versatile 2D supramolecular materials.

## Results and Discussion

**Design of cation- $\pi$  monomers.** Scheme 1a shows the molecular structure of monomers towards the formation of 2DSOLs. The monomer (cation1 $\pi$ 1)<sub>3</sub> has C<sub>3</sub> symmetry and consists of a non-aromatic triazine core and three arms.



**Scheme 1. Schematic illustration of formation process of 2D supramolecular organic layers.** (a) Mixed monomers; (b) Structure stabilized by double cation- $\pi$  interaction; (c) Assembled fragment further interconnected to form ordered 2D supramolecular organic layers with internal ordered structure; (d) A proposed [6 + 6] hexagonal macrocycle unit.

The core structure helps avoid any unfavorable cation- $\pi$  interactions; each arm comprises of a peripheral indole unit ( $\pi$ 1) and a diethyl imidazolium salt moiety (cation1). The  $C_2$  symmetric (cation2 $\pi$ 2)<sub>2</sub> monomer composes of a biphenyl group ( $\pi$ 2) and two alkali metal cations (Na<sup>+</sup> or K<sup>+</sup>, cation2-1 or cation2-2). Notably, the cation- $\pi$  interaction possesses the self-sorting recognition effect,<sup>[17, 18]</sup> i.e., the cation-containing or conjugated  $\pi$ -containing groups can be endowed with the ability to associate with the most adaptable chemical group within a complex mixture.<sup>[10a, 12c]</sup> Specifically to the monomers studied, cation2 has a stronger specific affinity with  $\pi$ 1 than with  $\pi$ 2,<sup>[10a, 19]</sup> whereas the affinity between cation1 and  $\pi$ 2 is greater than that between cation1 and  $\pi$ 1.<sup>[20]</sup> Thus, on mixing of (cation1 $\pi$ 1)<sub>3</sub> with (cation2 $\pi$ 2)<sub>2</sub>, cation1- $\pi$ 2 and cation2- $\pi$ 1 were specifically recognized and associated (Scheme 1b). The cation1- $\pi$ 2 and cation2- $\pi$ 1 stabilized assemblies further interconnected to form a rigid, hexagonally patterned 2D structure (Scheme 1c). In order to prove the design rationale, we synthesized a series of monomers including (cation1 $\pi$ 1)<sub>3</sub>, (cation2-1 $\pi$ 2)<sub>2</sub>, and (cation2-2 $\pi$ 2)<sub>2</sub> as building blocks for the preparation of the proposed 2DSOLs (Scheme S1). Detailed synthetic procedures and characterization results were shown in the Supporting Information, Sections 3 and 9.

**Formation of 2DSOLs.** In order to form a double cation- $\pi$  stabilized 2DSOLs, a controlled amount of (cation1 $\pi$ 1)<sub>3</sub> and (cation2 $\pi$ 2)<sub>2</sub> monomers were dissolved in a solution. Here, we used DMSO as the solvent. The solution was placed in a vacuum at 90 °C for 12 h. After evaporation of the solvent, 2D layers were simultaneously formed. The 2D layers obtained by mixing (cation1 $\pi$ 1)<sub>3</sub>-(cation2-1 $\pi$ 2)<sub>2</sub> and (cation1 $\pi$ 1)<sub>3</sub>-(cation2-2 $\pi$ 2)<sub>2</sub> were denoted as 2DSOL-1 and 2DSOL-2, respectively.

The structure, morphology, and composition of these two self-assemblies were similar, and therefore, we took 2DSOL-1 as a representative to demonstrate characterization. Transmission electron microscope (TEM) images revealed that 2DSOL-1 formed a thin and compact lamellated structure (Figures 1a). The lamellated structure was further confirmed by using high-angle annular dark-field scanning transmission electron microscopy (HAADF-STEM), as shown in Figure 1b. Furthermore, we employed energy dispersive X-ray spectroscopy (EDS) to characterize elemental distribution and found that the featured elements C, N, O, S, and Na of (cation1 $\pi$ 1)<sub>3</sub> and (cation2-1 $\pi$ 2)<sub>2</sub> were distributed uniformly throughout the entire layer. The surface composition of 2DSOL-1 and the oxidation states of surface elements were further investigated with X-ray photoelectron spectroscopy (XPS). As shown in Figure S4, all composition elements were found in the survey spectrum. The high-resolution Na 1s XPS showed the appearance of a single peak at a binding energy of 1071.34 eV suggesting the presence of Na (I).<sup>[21]</sup> The value of the binding energy is similar to the binding energy of Na (I) in (cation2-1 $\pi$ 2)<sub>2</sub> (Figure S2, 1071.26 eV), indicating that the chemical state of Na<sup>+</sup> did not change during the formation process of 2DSOL-1. An AFM image displayed that the thickness of the lamellate is around 4.2 ± 0.3 nm (Figure 1c). Additionally, the measurement of nitrogen gas absorption of 2DSOL-1 at 77 K did not yield a significant Brunauer-Emmett-Teller surface area, which may be attributed to the thin lamellated structure with open pores and the residue DMSO. The formation of 2DSOL-2 and the morphologies of 2DSOLs in solutions were also experimentally confirmed (Figures S1–S8). Summing up, the experimental characterizations indicate that the as-prepared 2DSOLs exhibit a compact, uniform, and lamellated structure. In order to test the structural stability of 2DSOL-1, we immersed the as-prepared 2DSOL-1 in DMSO; the solution was

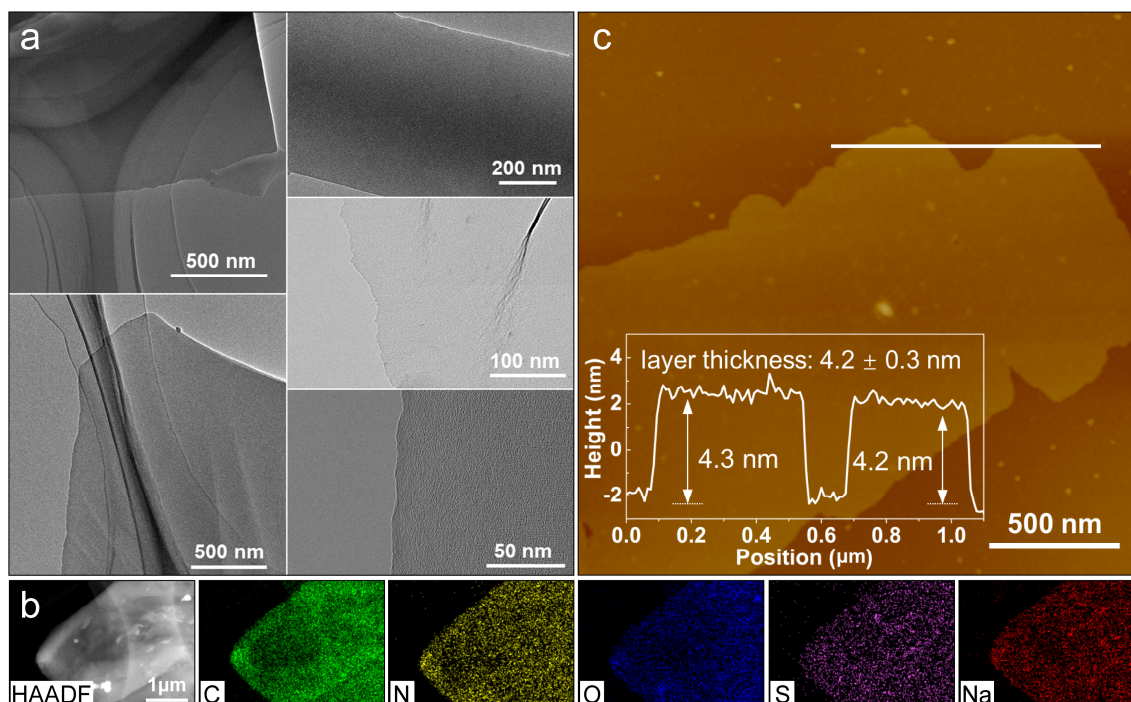


**Figure 1. Characterization of representative 2D supramolecular organic layers (2DSOL-1).** (a) TEM images with various magnifications; (b) HAADF-STEM image and EDS mapping; (c) AFM image of a layer and the corresponding height profiles (inset).

subsequently dried out. We repeated this process seven times. The lamellated structure and thickness of 2DSOL-1 did not change after seven cycles (Figure S9). In particular, the corresponding root-mean-square (RMS) remained between 0.20–0.37 nm, and the areas were maintained above 2  $\mu\text{m}^2$ .

#### Double cation- $\pi$ -driven self-assembly mechanism.

Considering the structural design, we speculated that the formation of a double cation- $\pi$  interaction ( $\text{Na}^+/\text{K}^+$ -indole, and imidazolium cation-biphenyl) is the pivotal factor to regulating the self-assembly process. We performed a series of experiments to testify this speculation. As shown in the  $^1\text{H}$  NMR titration experiments of  $(\text{cation}1\pi1)_3$  and  $(\text{cation}2-1\pi2)_2$  (Figure 2a), the  $(\text{cation}1\pi1)_3$  was gradually doped into a solution of  $(\text{cation}2-1\pi2)_2$  in  $\text{DMSO}-d_6$ , causing an upfield shift of the resonances  $\text{H}_a$  and  $\text{H}_b$  (protons from the imidazolium group of cation1), whereas a downfield shift of resonances  $\text{H}_1$  and  $\text{H}_2$  (protons from the biphenyl group of  $\pi2$ ) was observed. This result evidences a strong interaction between cation1 and  $\pi2$ . In addition, all  $^1\text{H}$  NMR signals broadened with increasing  $(\text{cation}1\pi1)_3$  concentration, indicating the formation of high-molecular-weight aggregates.<sup>[23]</sup>  $^{23}\text{Na}$  NMR titration further displayed that  $(\text{cation}2-1\pi2)_2$  had a Na peak at  $\delta = 0.41$  ppm in the absence of  $(\text{cation}1\pi1)_3$ . However, when  $(\text{cation}1\pi1)_3$  was gradually doped, the initial Na resonance yielded a small upfield shift ( $\Delta\delta = -0.44$  ppm, Figure 2b). A likely explanation is that the metal center of  $\text{Na}^+$  (cation2-1) was affected by a higher shielded environment with the addition of indole ( $\pi1$ ).<sup>[24]</sup> Small shifts from a  $\text{Na}^+$ -indole interaction cannot cause large perturbations to the electronic structure of the  $\text{Na}^+$ . At the same time, the existence of a  $\text{Na}^+$ -indole ( $\text{cation}2-1-\pi1$ ) interaction was also verified by  $^1\text{H}$ - $^1\text{H}$  nuclear Overhauser effect

spectroscopy (NOSEY) (Figure S13). Combined, these NMR results indicate that the so-called “double cation- $\pi$  interaction” plays a dominant important role in the self-assembly process.

We further used fluorescence titration experiments to confirm the cation- $\pi$  interaction. Figure 2c shows that the free  $(\text{cation}2-1\pi2)_2$  in DMSO displayed a strong emission peak at 331 nm. On gradual addition of  $(\text{cation}1\pi1)_3$  to the  $(\text{cation}2-1\pi2)_2$  solution, the fluorescence intensity gradually increased, accompanied by a bathochromic effect of the maximum emission peak (red arrow,  $\lambda_{\text{max}} = 331 \rightarrow 337$  nm). Mechanistically, the cation- $\pi$  interaction could contribute to the fluorogenicity by inhibiting the twisting motion of the indole and biphenyl groups.<sup>[25]</sup> On the other hand, the cation- $\pi$  interaction is complex, involving a partial charge transfer.<sup>[10a]</sup> On addition of  $(\text{cation}1\pi1)_3$  to the  $(\text{cation}2-1\pi2)_2$  solution, the UV-vis absorption intensity of the mixed solution increased significantly, accompanied by a bathochromic effect (Figure 2d). Importantly, a broad absorption hillock emerged at 320 to 400 nm for the mixed solution. We assigned the absorption hillock to a weak charge transfer between the donor ( $\pi1$  and  $\pi2$ ) and the acceptor (cation2-1 and cation1). The isothermal titration calorimetry experiments were applied to further quantify the strength of the cation- $\pi$  interactions between  $(\text{cation}1\pi1)_3$  and  $(\text{cation}2-1\pi2)_2$ . As shown in Figure S14, the association constant of  $(\text{cation}1\pi1)_3$ -Br and  $(\text{cation}2-1\pi2)_2$  was found to be  $K_a = 1.33 \times 10^4 \text{ M}^{-1}$ . The high association constant again verified the existence of a strong cation- $\pi$  interaction.<sup>[26]</sup> Similar results for  $(\text{cation}1\pi1)_3$  and  $(\text{cation}2-2\pi2)_2$  system can be found in the Supporting Information (Figures S15–S18). Additionally, the reversibility of the cation- $\pi$  interaction was also verified by alternatively adding trifluoroacetic acid and triethylamine to the

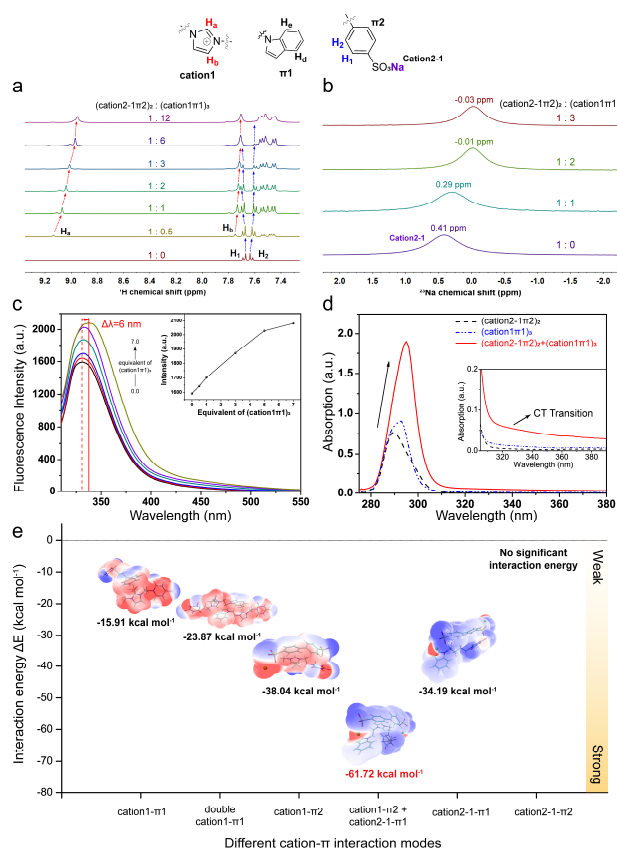


**Figure 2. Experimental and theoretical confirmation of the double cation- $\pi$  interaction in 2DSOL-1.** (a)  $^1\text{H}$  NMR titration experiments. Partial  $^1\text{H}$  NMR spectra (400 MHz, 25  $^\circ\text{C}$ ): (cation2-1 $\pi$ 2) $_2$  (3.0 mM) in DMSO- $d_6$  in the presence of 0–12.0 equiv. of (cation1 $\pi$ 1) $_3$ . (b)  $^{23}\text{Na}$  NMR titration experiments. (cation2-1 $\pi$ 2) $_2$  (20.8 mM) in DMSO- $d_6$  in the presence of 0–3.0 equiv. of (cation1 $\pi$ 1) $_3$ . (c) Fluorescence titration experiments. Fluorescence emission spectra of (cation2-1 $\pi$ 2) $_2$  (1  $\mu\text{M}$ ,  $\lambda_{\text{exc}}$  = 285 nm), and the insert showed a plot of fluorescence intensity at  $\lambda_{\text{max}}$  = 330 nm versus (cation1 $\pi$ 1) $_3$  equivalents; (d) UV-vis spectra for (cation2-1 $\pi$ 2) $_2$ , (cation1 $\pi$ 1) $_3$ , and a mixture solution of them (DMSO, [(cation2-1 $\pi$ 2) $_2$ ] = 1 mM, [(cation1 $\pi$ 1) $_3$ ] = 3 mM). (e) Energy distribution mapping of different cation- $\pi$  interactions via using the density functional theory calculation. The interaction energies  $\Delta E$  have been corrected for basis set superposition error (BSSE) by using the counterpoise method.<sup>[22]</sup> The image in the insert shows the molecular electrostatic potential mapping of cation- $\pi$  interactions (the color axis is removed for clarity, and the complete images were shown in Figures S29 and S30 in the Supporting Information).

mixed monomer solution. This is because the cation- $\pi$  interaction can be associated and dissociated at high and low pH values, respectively (Figure S19).<sup>[14b, 27]</sup>

A series of full-structure control experiments<sup>[28]</sup> were designed to investigate how each component group influences the self-assembly process. In doing so, we comparatively studied the AFM images of (cation1 $\pi$ 1) $_3$  and (cation2 $\pi$ 2) $_2$  (Figures S20–S25). Irregular aggregates were found (Figure S20), which might be attributed to the formation of non-optimized cation- $\pi$  interaction among monomers. This indicated that the self-sorting of cation- $\pi$  interaction is the key factor for the formation of 2DSOLs, which will be further verified by theoretical methods in the next paragraph. Further, irregular or spherical aggregates

were formed in the absence of cation1,  $\pi$ 1, cation2, or  $\pi$ 2 group (Figures S21–S24), indicating that the double cation- $\pi$  formation is indispensable for the formation of cation- $\pi$  driven 2D self-assembly. The self-assembly of similar symmetry monomers, e.g., (cation1 $\pi$ 1) $_2$  and (cation2 $\pi$ 2) $_2$  produced irregular aggregates (Figure S25), indicating that the imbalance is a premise for the regularity of 2D self-assembly. Additionally, to verify whether the movable Na $^+$ /K $^+$  (cation2) could be anchored near the indole ( $\pi$ 1), the unmovable ammonium (cation2-3) and Cs $^+$  ((cation2-4) that has a larger volume and a lower charge density than Na $^+$  or K $^+$ ) were prepared. The formation of lamellated structures (Figure S26) suggested that Na $^+$  can be anchored near the indole to provide an effective cation- $\pi$  interaction similar to the ammonium cation. Specifically, the Na $^+$  was disposed on the central axis of indole plane.<sup>[14b, 27]</sup> On the other hand, when Na $^+$  was replaced by Cs $^+$ , the formed lamellated structure was irregular (Figure S27). It is worth to mention that the thickness of 2DSOLs increased (4.2 < 4.6 < 5.5 nm) with increasing the size of the (cation2) (Na $^+$  < K $^+$  < Cs $^+$ ). Thus, the thickness of 2DSOLs could be effectively adjusted by using cations of different sizes.

DFT calculation was further employed to investigate the interaction energies of different cation- $\pi$  pairs.<sup>[14b, 15b]</sup> We first designed optimized molecular models of three monomers using the Gaussian 09 package (Figure S28). Since the three arms of (cation1 $\pi$ 1) $_3$  are identical, we only chose one of the arms to analyze the cation- $\pi$  interactions of the (cation2-1 $\pi$ 2) $_2$  pair. As shown in the energy distribution map, all possible cation- $\pi$  pairs were calculated (Figures 2e, S29, and S30). It was found that the interaction energy of cation1- $\pi$ 2 (–38.04 kcal mol $^{-1}$ ) was stronger than that of the energy of cation1- $\pi$ 1 (–15.91 kcal mol $^{-1}$ ). On the other hand, cation2-1- $\pi$ 1 possessed a stronger binding force (–34.19 kcal mol $^{-1}$ ) than cation2-1- $\pi$ 2. Thus, the results of DFT calculation coincide with the viewpoint of the aforementioned full-structure control experiments and further verify the significance of the competitive self-sorting recognition upon self-assembly. Note that the synergistic interaction energy (–61.72 kcal mol $^{-1}$ ) of the double cation- $\pi$  interaction from (cation1- $\pi$ 2 + cation2-1- $\pi$ 1) was much stronger than that of the double cation1- $\pi$ 1 interaction energy (–23.87 kcal mol $^{-1}$ ). In addition, we also found that the interaction energy of (cation1- $\pi$ 2 + cation2-1- $\pi$ 1) was slightly stronger than that of (cation1- $\pi$ 2 + cation2-2- $\pi$ 1) (–57.53 kcal mol $^{-1}$ , Figure S29b), indicating a better matching of cation2-1- $\pi$ 1 than cation2-2- $\pi$ 1.

Based on the analysis above, we explored the structure of the 2D self-assembly by using DMol3 model simulation in the Materials Studio Software. DMol3 model simulation indicated that the monomer could get together into a crooked hexagon, as shown in Figure 3b. A crooked molecular hexagon has three layers. The top and bottom layers consist of three (cation1 $\pi$ 1) $_3$  molecules that form a C $_3$ -symmetrical hexagonal macrocycle; the twist angle ( $\alpha$ ) was 60 $^\circ$  between the top and bottom macrocycles; the middle layer consists of six (cation2-1 $\pi$ 2) $_2$  molecules that act as linking units. The theoretically proposed structure was confirmed by using Small-angle X-ray scattering (SAXS) experiment. The SAXS results displayed a strong and sharp scattering peak corresponding to a  $d_1$  spacing of

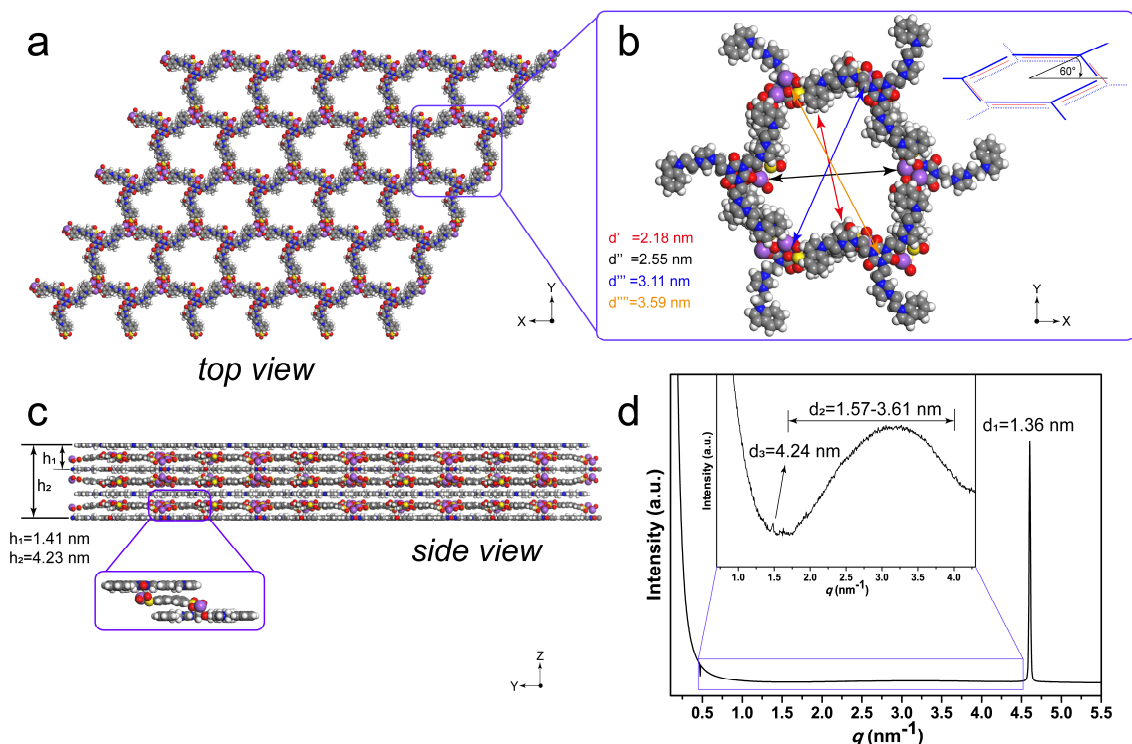


**Figure 3. Internal arrangement model and confirmation of 2DSOL-1.** (a) Top view of the arrangement model, capable of forming a 2D hexagonal array with alternatively stacking (cation1 $\pi$ 1)<sub>3</sub> and (cation2-1 $\pi$ 2)<sub>2</sub>; (b) Proposed hexagonal fragments; (c) Side view of the arrangement model. 2D hexagonal units also assembled in the vertical direction to form thin-layers with long-range ordering; the inset illustrates a proposed self-assembly mode between layers; (d) Synchrotron small-angle X-ray scattering of the 2DSOL-1 solid sample.

1.36 nm (Figure 3d), and the result matched well with the calculated thickness  $h_1$  (approximately 1.41 nm) of the “hexagonal fragment”, that is, the thickness of three stacked molecular layers, as shown in Figure 3c. A broad scattering peak corresponding to a  $d_2$  spacing of approximately 1.57–3.61 nm was assigned to the pore diameter of the irregular hexagon (Figure 3b). The broad scattering peak may be attributed to the overlap of multiple approximate scatterings of the irregular hexagon. Additionally, the broadening feature of the peak reasonably reflected the dynamic nature of 2DSOLs.<sup>[6e]</sup> A weak scattering peak corresponding to a  $d_3$  spacing of 4.24 nm denoted the thickness  $h_2$  (approximately 4.23 nm, Figure 3c) consisting of approximately three  $h_1$ . The results above were consistent with the layer thickness of 2DSOL-1 measured in an AFM image (approximately 4.2 nm, inset of Figure 1c). Therefore, all experimental results matched well with the calculated molecular packing model, confirming the rationale of the proposed segmental structure and the long-range periodicity of 2DSOL-1. Moreover, the anions  $\text{PF}_6^-$  nearby the imidazolium cation are located in the pores of the framework.

**Stability of 2DSOLs.** We examined the stability of the 2DSOLs. TGA results show that both 2DSOL-1 and 2DSOL-2 had a weight loss of only 10% at 290 °C and 317 °C, respectively (Figure S31b). Furthermore, to examine the levels of solvent resistance, the samples were immersed in methanol, ethanol, water, and dichloromethane for 4 days. We did not find any

visual changes on the uniformity, thickness, and RMS of the two examined 2DSOL samples (Figures S32–S33). Combined, these measurements indicate that 2DSOLs have excellent thermal stability and immeasurable level of solvent resistance.

**Catalytic activity of the 2DSOL/PdNPs hybrid.** The excellent stability allows the 2DSOLs to be used in real-world applications. Here, we demonstrated that the 2DSOLs can be used as nanoparticle carriers to catalyze a reaction that occurs on the surface of a nanoparticle. The advantage of using such carriers is to increase the surface area of the nanoparticle by eliminating the nanoparticle aggregation. To demonstrate the ability of 2DSOLs as a nanoparticle carrier, we loaded Pd nanoparticles (Pd NPs) onto the 2DSOLs and tested the catalytic activity of the resulting 2DSOL/NPs hybrid in the Suzuki–Miyaura coupling reaction (S–M reaction).

The preparation of the 2DSOL/PdNPs hybrid is described as follows: In order to disperse Pd NPs onto 2DSOLs, a slow reduction process was performed to reduce metal ions to zero-valent NPs. During this process, the nitrogen groups of the 2DSOLs provide an abundance anchor sites to nucleate the NPs, and the well-isolated pore channels confine the growth of the NPs. Thus, the aggregation of entrapped NPs can be minimized. The TEM image of the 2DSOL-2/PdNPs hybrid (Figure 4a) reveals that the ultra-small Pd NPs were uniformly

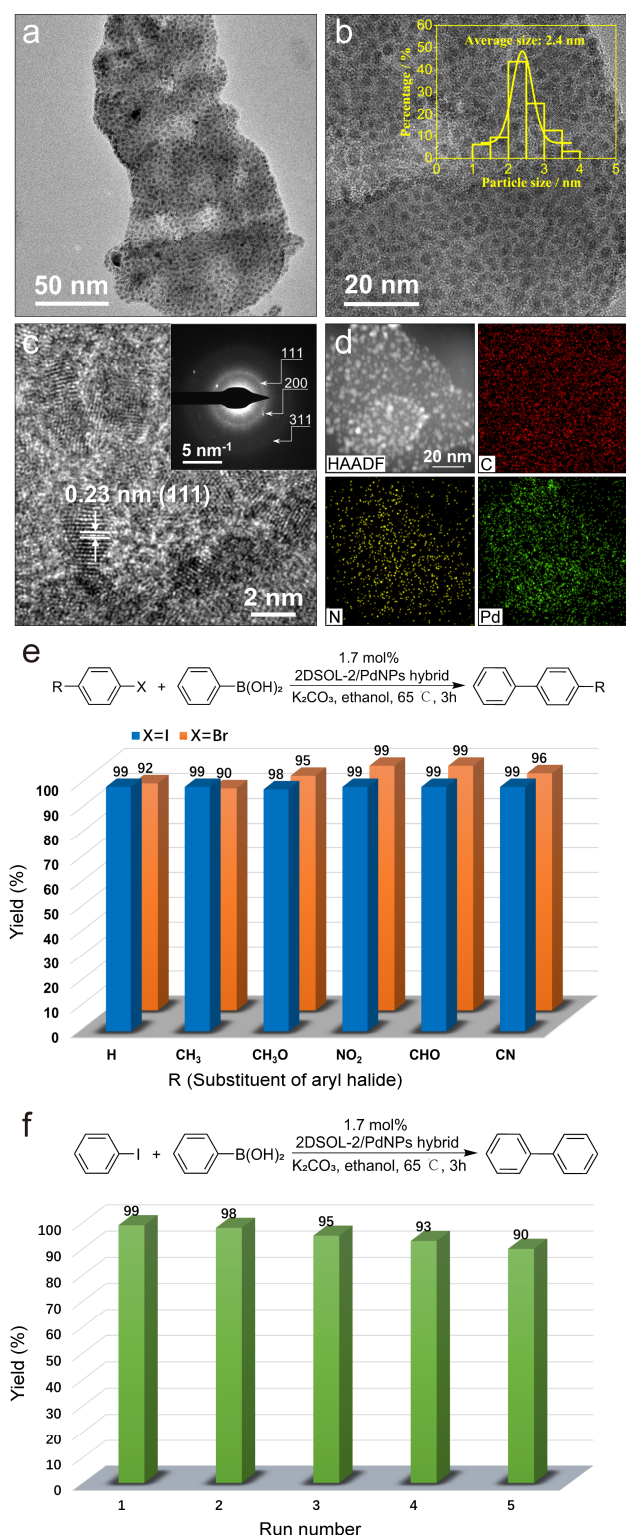


**Figure 4. Characterizations and catalytic activity of the 2DSOL-2/PdNPs hybrid.** (a) TEM image displays the stable layer structure and well-anchored Pd NPs; (b) high-magnification TEM image indicates the well-dispersed Pd NPs, and the inset shows the size distribution; (c) HR-TEM image presents the lattice fringes of Pd NPs, and the inset shows the corresponding SAED pattern; (d) HAADF-STEM and EDS mapping of feature element C, N, and Pd, respectively; (e) Catalytic activity in the S-M reaction. Isolated yields. (f) Reusability in the S-M reaction. Isolated yields.

distributed on the 2D layer. The high-magnification TEM image (Figure 4b) further displays that the well-dispersed and high density Pd NPs possess a narrow size distribution (inset in Figure 4b). As seen in the HR-TEM image (Figure 4c), the ordered and clear lattice fringes, and the interplanar  $d$ -spacing (0.23 nm) indicates the formation of Pd(0) nanoclusters oriented in the (111) plane. The lattice fringes of some Pd NPs were not clear. This is perhaps owing to the encapsulation of them within the hexagonal pores of 2D layer structure. The corresponding SAED pattern implied the polycrystalline nature of Pd NPs with (111), (200) and (311) orientations (inset in Figure 4c). The characteristic diffraction ring of (111) was consistent with the observation of PXRD (Figure S34). EDS elemental mapping indicated that the Pd, N and C elements are uniformly distributed throughout the whole layer (Figure 4d). Taken together, this data indicates that the 2DSOL-2/PdNPs hybrids were successfully prepared.

We examined the catalytic activity of 2DSOL-2/PdNPs in the S-M reaction, which is widely applied in fine-chemical and pharmaceutical synthesis.<sup>[29]</sup> The main results were displayed in Figure 4e, and the detail description is provided in the Supporting Information (Section 8.5). Despite the low dosage of the 2DSOL-2/PdNPs hybrid (1.7 mol%), a broad substrate suitability and excellent isolated yields for aryl iodides (>98% yields, blue histograms), and aryl bromides (>90% yields, orange histograms) under mild condition (65 °C, 3h) was exhibited. The 2DSOL-2/PdNPs hybrid also showed outstanding stability and recyclability. It was readily reused following centrifugation and washing with CH<sub>2</sub>Cl<sub>2</sub> without any additional reactivation process. The specific reaction scheme is illustrated in Figure 4f. The results demonstrated that the isolated yields of catalytic products attained remains over 90% after four-times reusing of the 2DSOL-2/PdNPs hybrid. The morphology and size of 2DSOL-2/PdNPs hybrid was retained after multiple reuses (Figure S39). The catalytic experiment evidently indicated that the 2DSOLs can act as the carrier of nanoparticles and thus eliminate aggregation.

## Conclusion

We purposed a double cation- $\pi$ -driven strategy to prepare 2D self-assembly. The double cation- $\pi$  interaction was generated based on the competitive self-sorting recognition of two kinds of unbalanced hetero-complementary monomers comprising of cations and aromatic groups. The obtained 2D self-assemblies could be used to load Pd nanoparticles and the resulting hybrid exhibited superior catalytic performance relative to the dispersed nanoparticle catalysts towards reactions that necessitate surface catalysis. We believe that such a double cation- $\pi$ -driven strategy is a new rationale towards the precise preparation of 2D self-assemblies and overcomes a long-standing challenge in regard to the fabrication of 2D stable supramolecular materials.

## Acknowledgements

This work was supported by the National Science Foundation of China (No. 21674086 and 21873094), Natural Science Basic Research Plan in Shaanxi Province of China (2018JZ2003), the

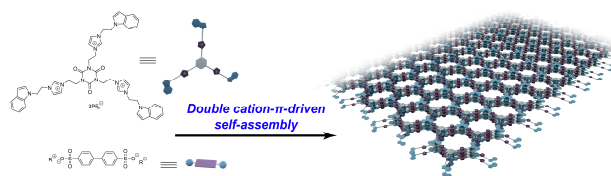
Fundamental Research Funds for the Central Universities (3102019PY003), the student innovation fund of Northwestern Polytechnical University (201910699027), and Key Research Program of Frontier Sciences, Chinese Academy of Sciences (ZDBS-LY-SLH033). We would like to thank the Analytical & Testing Center of Northwestern Polytechnical University for electron microscope, Prof. Feng Liu (Xi'an Jiaotong University) for the synchrotron SAXS, and Prof. Liping Cao (Northwest University) for the ITC tests. We also thank Prof. Peng Yang (Shaanxi Normal University) and Prof. Daoyong Chen (Fudan University) for their useful suggestions.

**Keywords:** cation- $\pi$  interaction • supramolecular self-assembly • supramolecular chemistry

- [1] a) A. K. Geim, K. S. Novoselov, *Nat. Mater.* **2007**, *6*, 183-191; b) C. Tan, X. Cao, X.-J. Wu, Q. He, J. Yang, X. Zhang, J. Chen, W. Zhao, S. Han, G.-H. Nam, M. Sindoro, H. Zhang, *Chem. Rev.* **2017**, *117*, 6225-6331; c) F. Yang, S. Cheng, X. Zhang, X. Ren, R. Li, H. Dong, W. Hu, *Adv. Mater.* **2018**, *30*, 1702415.
- [2] a) R. Dong, T. Zhang, X. Feng, *Chem. Rev.* **2018**, *118*, 6189-6235; b) X. Zhuang, Y. Mai, D. Wu, F. Zhang, X. Feng, *Adv. Mater.* **2015**, *27*, 403-427; c) S.-L. Cai, W.-G. Zhang, R. N. Zuckermann, Z.-T. Li, X. Zhao, Y. Liu, *Adv. Mater.* **2015**, *27*, 5762-5770.
- [3] a) J. D. Cojal González, M. Iyoda, J. P. Rabe, *Nat. Commun.* **2017**, *8*, 14717; b) J. Zhang, H. Geng, T. S. Virk, Y. Zhao, J. Tan, C.-a. Di, W. Xu, K. Singh, W. Hu, Z. Shuai, Y. Liu, D. Zhu, *Adv. Mater.* **2012**, *24*, 2603-2607; c) W. Zhu, R. Zheng, X. Fu, H. Fu, Q. Shi, Y. Zhen, H. Dong, W. Hu, *Angew. Chem. Int. Ed.* **2015**, *54*, 6785-6789; d) N. Seiki, Y. Shoji, T. Kajitani, F. Ishiwari, A. Kosaka, T. Hikima, M. Takata, T. Someya, T. Fukushima, *Science* **2015**, *348*, 1122-1126; e) W. Yao, Y. Yan, L. Xue, C. Zhang, G. Li, Q. Zheng, Y. S. Zhao, H. Jiang, J. Yao, *Angew. Chem. Int. Ed.* **2013**, *52*, 8713-8717; f) L. Yue, S. Wang, D. Zhou, H. Zhang, B. Li, L. Wu, *Nat. Commun.* **2016**, *7*, 10742.
- [4] a) X. He, M.-S. Hsiao, Charlotte E. Boott, Robert L. Harniman, A. Nazemi, X. Li, Mitchell A. Winnik, I. Manners, *Nat. Mater.* **2017**, *16*, 481-488; b) K. T. Nam, S. A. Shelby, P. H. Choi, A. B. Marciel, R. Chen, L. Tan, T. K. Chu, R. A. Mesch, B.-C. Lee, M. D. Connolly, C. Kisielowski, R. N. Zuckermann, *Nat. Mater.* **2010**, *9*, 454-460; c) Y. Wei, J. Tian, Z. Zhang, C. Zhu, J. Sun, Z. Li, *Macromolecules* **2019**, *52*, 1546-1556; d) R. V. Mannige, T. K. Haxton, C. Proulx, E. J. Robertson, A. Battigelli, G. L. Butterfoss, R. N. Zuckermann, S. Whitelam, *Nature* **2015**, *526*, 415-420.
- [5] a) M. Moradi, L. G. Tulli, J. Nowakowski, M. Baljovic, T. A. Jung, P. Shahgaldian, *Angew. Chem. Int. Ed.* **2017**, *56*, 14395-14399; b) T. Kambe, R. Sakamoto, K. Hoshiko, K. Takada, M. Miyachi, J.-H. Ryu, S. Sasaki, J. Kim, K. Nakazato, M. Takata, H. Nishihara, *J. Am. Chem. Soc.* **2013**, *135*, 2462-2465; c) R. Dong, M. Pfeffermann, H. Liang, Z. Zheng, X. Zhu, J. Zhang, X. Feng, *Angew. Chem. Int. Ed.* **2015**, *54*, 12058-12063; d) T. Bauer, Z. Zheng, A. Renn, R. Enning, A. Stemmer, J. Sakamoto, A. D. Schlüter, *Angew. Chem. Int. Ed.* **2011**, *50*, 7879-7884.
- [6] a) K.-D. Zhang, J. Tian, D. Hanifi, Y. Zhang, A. C.-H. Sue, T.-Y. Zhou, L. Zhang, X. Zhao, Y. Liu, Z.-T. Li, *J. Am. Chem. Soc.* **2013**, *135*, 17913-17918; b) Y. Li, Y. Dong, X. Miao, Y. Ren, B. Zhang, P. Wang, Y. Yu, B. Li, L. Isaacs, L. Cao, *Angew. Chem. Int. Ed.* **2018**, *57*, 729-733; c) L. Zhang, Y. Jia, H. Wang, D.-W. Zhang, Q. Zhang, Y. Liu, Z.-T. Li, *Polym. Chem.* **2016**, *7*, 1861-1865. d) S.-Q. Xu, X. Zhang, C.-B. Nie, Z.-F. Pang, X.-N. Xu, X. Zhao, *Chem. Commun.* **2015**, *51*, 16417-16420; e) L. Zhang, T.-Y. Zhou, J. Tian, H. Wang, D.-W. Zhang, X. Zhao, Y. Liu, Z.-T. Li, *Polym. Chem.* **2014**, *5*, 4715-4721.
- [7] a) B. Narayan, S. P. Senanayak, A. Jain, K. S. Narayan, S. J. George, *Adv. Funct. Mater.* **2013**, *23*, 3053-3060; b) S. Ghosh, D. S. Philips, A. Saeki, A. Ajayaghosh, *Adv. Mater.* **2017**, *29*, 1605408; c) M. Vyborny, A. V. Rudnev, S. M. Langenegger, T. Wandlowski, G. Calzaferri, R. Häner, *Angew. Chem. Int. Ed.* **2013**, *52*, 11488-11493.
- [8] a) S. Wiegold, J. Li, P. Simon, M. Krause, Y. Avlasevich, C. Li, J. A. Garrido, U. Heiz, P. Samorì, K. Müllen, F. Esch, J. V. Barth, C.-A. Palma, *Nat. Commun.* **2016**, *7*, 10700; b) R. Makiura, K. Tsuchiyama, E. Pohl, K. Prassides, O. Sakata, H. Tajiri, O. Kononov, *ACS Nano* **2017**, *11*, 10875-10882; c) J. Chen, E. Zhu, J. Liu, S. Zhang, Z. Lin, X. Duan, H. Heinz, Y. Huang, J. J. De Yoreo, *Science* **2018**, *362*, 1135.
- [9] a) M. B. Avinash, T. Govindaraju, *Adv. Funct. Mater.* **2011**, *21*, 3875-3882; b) Z.-Q. Lin, J. Liang, P.-J. Sun, F. Liu, Y.-Y. Tay, M.-D. Yi, K. Peng, X.-H. Xia, L.-H. Xie, X.-H. Zhou, J.-F. Zhao, W. Huang, *Adv. Mater.* **2013**, *25*, 3664-3669; c) L. Han, M. Wang, X. Jia, W. Chen, H. Qian, F. He, *Nat. Commun.* **2018**, *9*, 865.
- [10] a) J. C. Ma, D. A. Dougherty, *Chem. Rev.* **1997**, *97*, 1303-1324; b) A. S. Mahadevi, G. N. Sastry, *Chem. Rev.* **2013**, *113*, 2100-2138.
- [11] a) D. A. Dougherty, D. A. Stauffer, *Science* **1990**, *250*, 1558; b) D. A. Stauffer, R. E. Barrans, D. A. Dougherty, *J. Org. Chem.* **1990**, *55*, 2762-2767.
- [12] a) J. P. Gallivan, D. A. Dougherty, *Proc. Natl. Acad. Sci. U. S. A.* **1999**, *96*, 9459; b) W. Di, Q. Hu, Z. Yan, W. Chen, C. Yan, X. Huang, J. Zhang, P. Yang, H. Deng, J. Wang, X. Deng, Y. Shi, *Nature* **2012**, *484*, 214; c) Q. Lu, D. X. Oh, Y. Lee, Y. Jho, D. S. Hwang, H. Zeng, *Angew. Chem.* **2013**, *125*, 4036-4040.
- [13] a) C. R. Kennedy, S. Lin, E. N. Jacobsen, *Angew. Chem. Int. Ed.* **2016**, *55*, 12596-12624; b) L. J. Juszcak, A. S. Eisenberg, *J. Am. Chem. Soc.* **2017**, *139*, 8302-8311.
- [14] a) Y.-M. Zhang, W. Zhu, W.-J. Qu, K.-P. Zhong, X.-P. Chen, H. Yao, T.-B. Wei, Q. Lin, *Chem. Commun.* **2018**, *54*, 4549-4552; b) G. Chang, L. Yang, J. Yang, M. P. Stoykovich, X. Deng, J. Cui, D. Wang, *Adv. Mater.* **2018**, *30*, 1704234.
- [15] a) S. Roy, S. P. Mondal, S. K. Ray, K. Biradha, *Angew. Chem. Int. Ed.* **2012**, *51*, 12012-12015; b) D. Wei, F. Ma, R. Wang, S. Dou, P. Cui, H. Huang, J. Ji, E. Jia, X. Jia, S. Sajid, A. M. Elseman, L. Chu, Y. Li, B. Jiang, J. Qiao, Y. Yuan, M. Li, *Adv. Mater.* **2018**, *30*, 1707583; c) Q. Zhang, S. Zhang, X. Zhang, L. Lei, W. Ma, C. Ma, L. Song, J. Chen, B. Pan, B. Xing, *Environ. Sci. Technol.* **2017**, *51*, 13659-13667.
- [16] L. Chen, G. Shi, J. Shen, B. Peng, B. Zhang, Y. Wang, F. Bian, J. Wang, D. Li, Z. Qian, G. Xu, G. Liu, J. Zeng, L. Zhang, Y. Yang, G. Zhou, M. Wu, W. Jin, J. Li, H. Fang, *Nature* **2017**, *550*, 380.
- [17] a) M. B. Avinash, P. K. Samanta, K. V. Sandeepa, S. K. Pati, T. Govindaraju, *Eur. J. Org. Chem.* **2013**, *2013*, 5838-5847; b) H. Li, X. Fan, X. Shang, M. Qi, H. Zhang, W. Tian, *Polym. Chem.* **2016**, *7*, 4322-4325; c) H. Li, X. Fan, M. Qi, Z. Yang, H. Zhang, W. Tian, *Chem. - Eur. J.* **2016**, *22*, 101-105.
- [18] M. M. Safont-Sempere, G. Fernández, F. Würthner, *Chem. Rev.* **2011**, *111*, 5784-5814.
- [19] S. L. Scherer, A. L. Stewart, R. C. Fortenberry, *Comput. Biol. Chem.* **2018**, *72*, 11-15.
- [20] J. A. Carrazana-García, E. M. Cabaleiro-Lago, J. Rodríguez-Otero, *Phys. Chem. Chem. Phys.* **2017**, *19*, 10543-10553.
- [21] C. D. Wagner, W. M. Riggs, L. E. Davis, J. F. Moulder, and G. E. Muilenberg in *Handbook of X-ray Photoelectron Spectroscopy*, Perkin-Elmer Corp., Minnesota, **1979**, pp. 55344.
- [22] S. F. Boys, F. Bernardi, *Mol. Phys.* **1970**, *19*, 553-566.
- [23] B. Song, Z. Wang, S. Chen, X. Zhang, Y. Fu, M. Smet, W. Dehaen, *Angew. Chem.* **2005**, *117*, 4809-4813.
- [24] a) A. Wong, R. D. Whitehead, Z. Gan, G. Wu, *J. Phys. Chem. A* **2004**, *108*, 10551-10559; b) D. L. Bryce, S. Adiga, E. K. Elliott, G. W. Gokel, *J. Phys. Chem. A* **2006**, *110*, 13568-13577.
- [25] a) Y. Liu, K. Miao, N. P. Dunham, H. Liu, M. Fares, A. K. Boal, X. Li, X. Zhang, *Biochemistry* **2017**, *56*, 1585-1595; b) I. Richter, J. Minari, P. Axe, J. P. Lowe, T. D. James, K. Sakurai, S. D. Bull, J. S. Fossey, *Chem. Commun.* **2008**, 1082-1084.
- [26] B. Qi, X. Guo, Y. Gao, D. Li, J. Luo, H. Li, S. A. Eghtesadi, C. He, C. Duan, T. Liu, *J. Am. Chem. Soc.* **2017**, *139*, 12020-12026.
- [27] L. Yang, M. Du, S. Yang, W. Wei, G. Chang, *Macromol. Rapid Commun.* **2018**, *39*, 1800031.
- [28] W. Bai, Z. Jiang, A. E. Ribbe, S. Thayumanavan, *Angew. Chem. Int. Ed.* **2016**, *55*, 10707-10711.
- [29] N. Miyaura, A. Suzuki, *Chem. Rev.* **1995**, *95*, 2457-2483.

## Entry for the Table of Contents

We propose a “double cation- $\pi$ -driven” strategy to prepare 2D supramolecular polymers with long-range ordered molecular hollow hexagons. The double cation- $\pi$  interaction makes the 2D supramolecular polymers be stable.



Xuedong Xiao,<sup>a,\*</sup> Hongbo Chen,<sup>b,\*</sup>  
Xuxu Dong,<sup>a</sup> Dazhuo Ren,<sup>a</sup>  
Qiang Deng,<sup>a</sup> Dapeng Wang,<sup>b</sup>  
and Wei Tian<sup>a,\*</sup>

**Double Cation- $\pi$ -Driven Strategy  
Enabling Two-Dimensional  
Supramolecular Polymers as  
Efficient Catalyst Carriers**

Accepted Manuscript